




A low-voltage electro-ionic soft actuator based on graphene nanoplatelets-sulfonated cellulose nanowhisker combined with microfibrillated cellulose

Fan Wang^{1,*} , Lei Wang¹, Zhenyu Wu¹, and Wei Wang^{1,*}

¹ School of Mechanical Engineering, Zhejiang Sci-Tech University, Hangzhou 310018, China

Received: 11 October 2022

Accepted: 5 December 2022

Published online:
1 January 2023

© The Author(s), under exclusive licence to Springer Science+Business Media, LLC, part of Springer Nature 2022

ABSTRACT

Low-voltage soft actuators with large displacement, long actuation durability, and fast response time have aroused great attention in soft robotics, wearable devices, haptic devices, and implantable or disposal biomedical devices. Herein, we report a low-voltage electroactive ionic soft actuator based on the sulfonated cellulose nanowhisker (SCN), microfibrillated cellulose (MFC), ionic liquids (IL), and graphene nanoplatelet (GN). The proposed SCN/MFC-IL-GN (0.1wt%) actuator demonstrated a large bending displacement (6.6 mm under ± 1 V sinusoidal input signal at 0.1 Hz, low driving voltage (as low as 0.25 V), wide actuation frequency (0.1 to 5.0 Hz), and long actuation durability (96.7% retention for 1 h), all of which stemmed from the strong crosslinking and ionic interactions among the functional sulfonated groups of SCN, hydroxyl groups of MFC, IL, and GN. Furthermore, the designed actuator was successfully employed to imitate the human finger's behaviors including turning on/off the flashlight and sliding electronic photographs on a smart phone screen. Therefore, the proposed SCN/MFC-IL-GN actuator has great potential in artificial muscles, soft robots, haptic devices, and wearable devices because of its low excitation voltage, large bending displacement, long actuation durability, and biofriendly property.

Introduction

In recent years, soft robots have attracted increasing interests because of the limitation of traditional robots, which are made of rigid connections and

joints [1–7]. Soft actuators play significant roles in achieving high-performance soft robots. Electroactive polymer (EAP), a new type of smart polymer material, can exhibit a bending deformation under the external electric field, which has good electrochemical and mechanical properties [8–13]. As a typical soft

Handling Editor: Stephen Eichhorn.

Address correspondence to E-mail: fwang@zstu.edu.cn; wangw@zstu.edu.cn

actuator, EAP has many advantages such as high flexibility, lightweight, low excitation voltage, and relatively large bending deformation. According to these unique properties, it can be applied to biomimetic robots, flexible/soft robots, wearable devices, and biomedical instruments [14–24]. However, some human friendly devices will require high-performance soft actuators with biofriendly properties.

Cellulose is the most abundant natural polymer and it can be produced from the wood, cotton, and other plants. The cellulose-based electroactive polymer actuator displayed the bending deformation at a low actuation voltage [25, 26]. Mahadeva et al. reported a cellulose–polypyrrole–ionic liquid nanocomposite that could exhibit actuation displacement in humidity environments [27]. Wang et al. introduced an electroactive paper prepared with cellulose and chitosan [28]. Hong et al. developed a highly porous ionic actuator based on polyaniline nanoparticles and cellulose acetate by using the electrospinning method [29]. However, these cellulose-based actuators showed low specific capacitances and poor conductivity, which lead to the small tip displacement, large actuation voltage, and slow response speed, resulting from the limitation of ionic transportation inside these membranes.

Recently, sulfonated cellulose nanowhisker (SCN) has attracted increasing attention because of its excellent emulsion stability, high biodegradability, biocompatibility, non-toxicity, high strength, and low cost [30, 31]. SCN is a needle-like nanomaterial obtained from the natural cellulose by acid or alkali treatment, and it can be well dispersed in water due to the presence of sulfonated groups ($-\text{SO}_3\text{H}$) on SCN surfaces. More interestingly, the sulfonated groups can be employed as protonation-active sites, resulting in the enhanced ion migration inside the membrane. Also, these sulfonated groups of SCN allow it to be functionalized with other active materials, including conducting polymers and ionic liquids. A uniform SCN membrane can be easily prepared by using a casting method, because SCN is present in water in the form of individual nanofibers. But the SCN membrane is brittle, which is not suitable for developing high-performance soft actuator. Microfibrillated cellulose (MFC) displayed similar properties with SCN, but showed large diameter and long length. MFC is usually used as a reinforcing agent in fabricating membranes, films, and nanocomposites [32, 33]. Furthermore, SCN and MFC can form a

strong crosslinking between sulfonated groups of SCN and hydroxyl groups of MFC. However, to the best of our knowledge, the use of SCN and MFC for developing high-performance ionic soft actuators has not been investigated.

In this study, we report a low-voltage electro-ionic actuator based on biofriendly SCN, MFC, graphene nanoplatelet (GN), and ionic liquid (IL, [EMIM][BF₄]). GN has received great attention owing to its excellent conductivity, outstanding chemical stability, superior mechanical strength, light weight, and low cost [34–36]. The SCN/MFC-IL-GN composite membrane was fabricated based on the SCN/MFC composite fibers by doping GN and IL. Furthermore, the flexible and biofriendly PEDOT:PSS (Poly (3,4-ethylenedioxythiophene)-poly (styrenesulfonate)) was used as electrodes by coating them on the membrane surfaces, as shown in Fig. 1. PEDOT:PSS is a non-metallic electrode, which has attracted people's interests because of its excellent biocompatibility and biodegradability, high conductivity, easy fabrication, and low cost [37–39]. Remarkably, the proposed SCN/MFC-IL-GN actuator exhibited excellent actuation performances under low driving voltages, which resulted from the strong crosslinking and ionic interactions among SCN/MFC, IL, and GN. More importantly, we successfully used the designed ionic actuator to imitate the human finger's behaviors including the turning on/off the flashlight and sliding electronic photographs on a mobile phone screen.

Experimental section

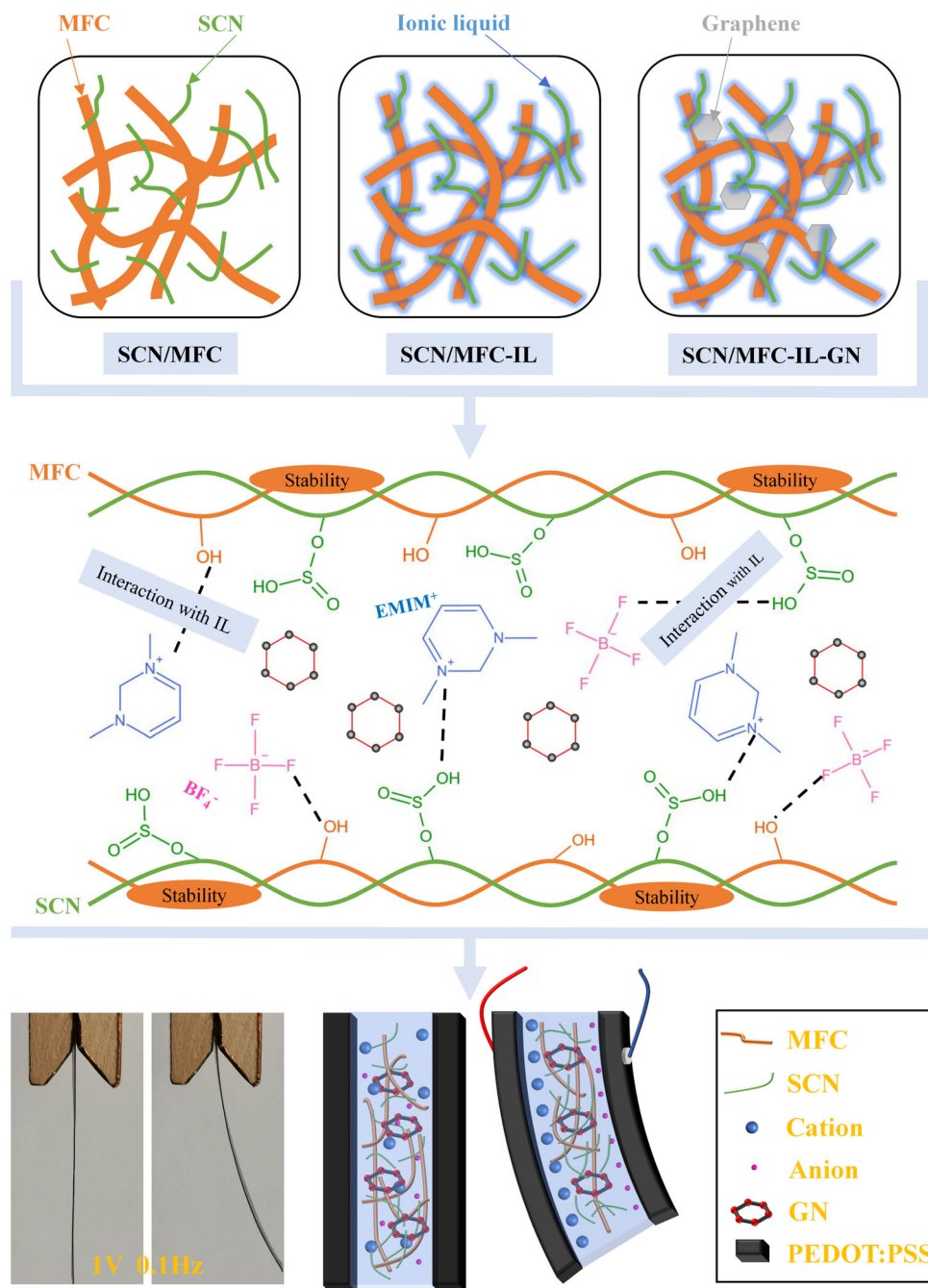
Materials

SCN (density 5.6%), MFC (density 1.85%), PEDOT:PSS (dark blue liquid, 1.3 wt% H₂O), and 1-ethyl-3-methylimidazolium tetrafluoroborate (EMIMBF₄; assay: 98%) were obtained from Sigma-Aldrich. Graphene nanoplatelets were received from GRAPHENE SUPERMARKET, USA.

Preparation of the SCN/MFC-IL-GN membrane

The SCN/MFC-IL-GN composite membrane was prepared by using a solution casting method. Firstly, the transparent aqueous dispersion of the SCN/MFC

Figure 1 Chemical structure and interactions of the SCN/MFC-IL-GN composite membrane; the actuation mechanism of the SCN/MFC-IL-GN ionic soft actuator.



mixture was prepared by mixing 7 g SCN and 4 g MFC at 50 °C. Secondly, the GN and SCN/MFC dispersions were mixed together in two mixing proportions, 0.05 wt% and 0.1 wt%, followed by stirring for 4 h at room temperature. Subsequently, 1 g IL was added to the SCN/MFC-GN mixture. The SCN/MFC-IL-GN was well dispersed by using ultrasound for 2 h. The bubbles in the mixing dispersions were removed by a vacuum oven. After the dispersion was poured into a casting mold and then dried in a

vacuum oven at 65 °C for 10 h, finally the SCN/MFC-IL-GN composite membrane was obtained.

Fabrication of the SCN/MFC-IL-GN actuator

The PEDOT:PSS solution was deposited on both surfaces of the composite membrane by a dip-coating method. The composite membrane was immersed in the solution for 5 min. The SCN/MFC-IL-GN

actuator was finally obtained after drying it in a vacuum oven at 50 °C for 4 h.

Characterization techniques

The surface and cross-sectional images of the samples were observed by using a scanning electron microscope (SEM) (GeminiSEM 500, ZEISS company). The chemical interaction and crystallinity of the samples were tested by a Nicolet iS-20 Fourier transform infrared spectrometer (FT-IR) (Thermo Fisher Scientific company) and high-resolution D8 discover X-ray diffractometer (XRD) (BRUKER AXS GMBH company), respectively.

We further measured the cyclic voltammetry (CV) curves of the actuators based on an electrochemical workstation. The specific capacitances were determined according to the following equation:

$$\text{Specific capacitance} = \frac{1}{\Delta V \cdot v \cdot S} \int_{V_1}^{V_2} I dV \quad (1)$$

where ΔV , v , and S were the potential window, scan rate, and surface area of the actuator, respectively.

Actuation performances

We measured tip displacements of the actuator ($40 \times 8 \times 0.28$ mm) based on a testing system consisting of a signal generator (33500B, Keysight Tech Co.), a laser displacement sensor (IL-300, KEYENCE Co.), and a power amplifier (FPA2000, Feel Tech Co.). One end of the actuator was fixed and the free length was 30 mm. The displacement data were obtained based on the processing system (NI Pxl-1078, National Instruments Co.) and LabVIEW program. The generated strain of the actuator was calculated by employing the following equation:

$$\varepsilon = 2dt / (d^2 + l^2) \quad (2)$$

where ε was the generated strain; d , t , and l were the displacement, thickness, and free length of the actuator, respectively.

Results and discussion

FE-SEM

SEM was used to observe the surface structures of the SCN/MFC-IL-GN membranes. As shown in Fig. 2a, for the pure SCN membrane, a large number of fibers

were observed in a random and tight distribution. The SCN/MFC membrane exhibited significantly larger fibers than the pure SCN membrane (Fig. 2b). The SCN/MFC composite fiber displayed a strong crosslinking due to the hydrogen bond formed by the sulfonic group in SCN and the hydroxyl group in MFC. As a result, the plasticity of the composite membrane increased. As shown in Fig. 2c, the IL was uniformly attached to the fibers, which was mainly attributed to the effective combination of BF_4^- of IL with sulfonic and hydroxyl groups in celluloses. Figure 2d exhibits that GN was embedded in cellulose due to the strong crosslinking of cellulose nanofibers with GN. Figure 2e and f demonstrates that PEDOT:PSS layers were well adhered to the surfaces of the SCN/MFC-IL-GN membrane, which played a significant role in achieving durable ionic actuators. Additionally, the average thicknesses of the top and bottom electrode layers and electrolyte layer were 22.7 μm , 17.6 μm , and 156.2 μm , respectively. Furthermore, the AFM images (Fig. 2g-i) proved the strong crosslinking of SCN/MFC nanofibers with GN. These results confirm the effective and strong interactions and crosslinking among SCN, MFC, IL, and GN.

XRD

Figure 3a shows the X-ray diffraction analysis of the composite membranes, which confirmed the influence of IL and GN on the crystallinity of the membranes. For the SCN and SCN/MFC composite membranes, two distinct diffraction peaks appeared at 2θ values of 15.7° and 23.1° , which proved the obvious evidence of the semi-crystalline nature of the composite membrane. After the addition of IL and GN, two new characteristic peaks were observed, indicating that the addition of IL and GN could maintain the properties of the SCN. Compared with the pure SCN membrane, the crystallinity of the SCN/MFC composite membrane was slightly reduced, which was the proof of MFC plasticization. With the addition of IL, the diffraction peak at approximately $2\theta = 14.6^\circ$ decreased slightly in comparison with that of the pure SCN membrane, showing that the crosslinking among SCN, MFC, and IL reduced the crystallinity of the composite membrane. Furthermore, sharp diffraction peaks appeared at $2\theta = 26.6^\circ$ and $2\theta = 54.7^\circ$, and the peak value of diffraction peaks increased with the

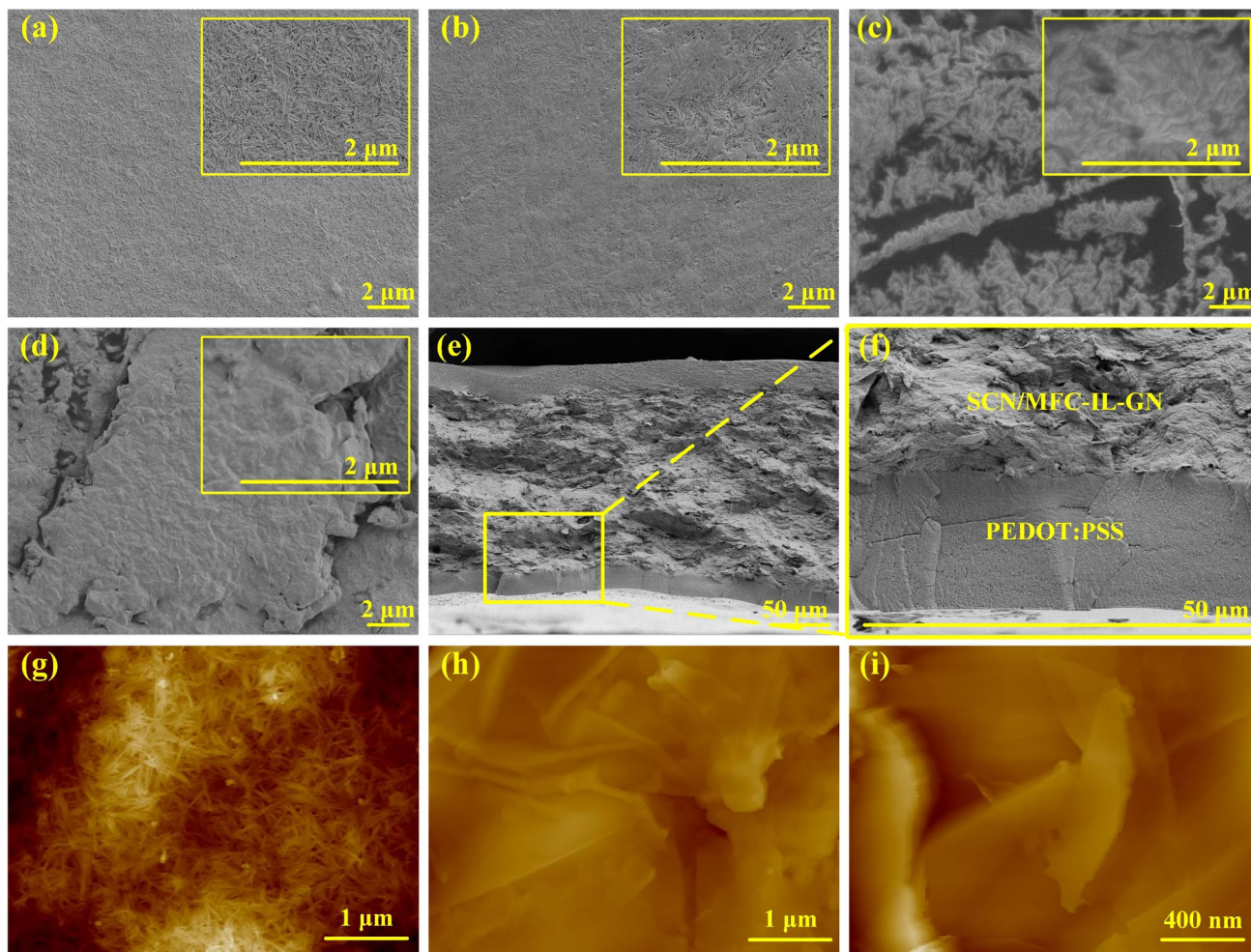


Figure 2 a–d Surface images of the pure SCN, SCN/MFC, SCN/MFC-IL, SCN/MFC-IL-GN membranes. e Cross-sectional image of the SCN/MFC-IL-GN ionic actuator. f Magnified cross-

sectional image of the actuator. g–h AFM images of the SCN/MFC and SCN/MFC-IL-GN membranes. i Magnified AFM image of the SCN/MFC-IL-GN membranes.

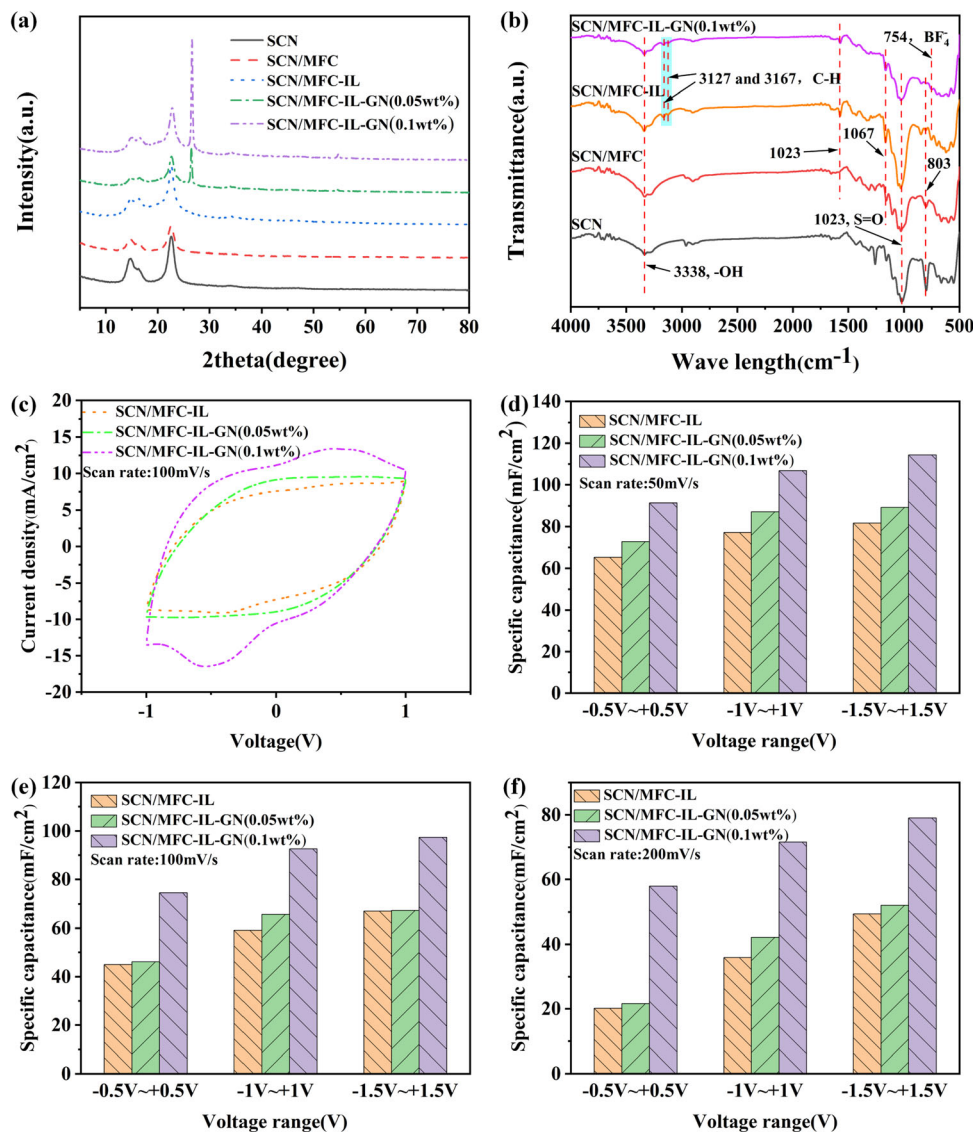
increment of GN concentration, which was mainly attributed to the strong interactions and crosslinking of SCN/MFC fibers with IL and GN.

FT-IR

Figure 3b displays FT-IR curves of the pure SCN, SCN/MFC, SCN/MFC-IL, and SCN/MFC-IL-GN membranes, confirming the strong crosslinking and ionic interactions among SCN, MFC, IL, and GN. In the curve of the SCN membrane, the characteristic peak corresponding to S = O in the $-\text{SO}_3\text{H}$ group appeared at 1023 cm^{-1} , and the stretching vibration peak of the $-\text{OH}$ group displayed at 3338 cm^{-1} . Compared with the pure SCN membrane, the intensity of the SCN/MFC membrane occurring at

3338 cm^{-1} (O–H stretching vibration) was enhanced, which was due to the strong crosslinking between SCN and MFC. For the SCN/MFC-IL membrane, basic peaks at 3127 cm^{-1} and 754 cm^{-1} corresponded to C–H and BF_4^- groups of IL. In the spectra of the SCN/MFC-IL-GN (0.1 wt%) membrane, the characteristic peaks at 1574 cm^{-1} , 1167 cm^{-1} , and 803 cm^{-1} became weaker, which was because of the interactions among SCN/MFC, IL, and GN. The hydrogen bond and electrostatic interaction between SCN/MFC and IL led to their uniform dispersion at the molecular level. These results demonstrate a strong crosslinking and ionic interactions among SCN/MFC fibers, IL, and GN.

Figure 3 **a** XRD pattern and **b** FT-IR curves of the SCN/MFC-IL-GN membranes. **c** CV curves of the SCN/MFC-IL-GN actuators under a scan rate of 100 mV/s. **d-f** Specific capacitances of the SCN/MFC-IL-GN actuators under different scan rates.



Cyclic voltammetric test

Furthermore, the cyclic voltammetry (CV) curves of the SCN/MFC-IL-GN ionic actuators were measured to study the charge dynamics and interfacial coupling of the actuator. Figure 3c displays the CV curves of the SCN/MFC-IL-GN actuators under a scan rate of 100 mV/s in the potential window of -1.0 to 1.0 V. The CV curve of the SCN/MFC-IL-GN (0.1wt%) actuator was approximately rectangular, indicating excellent charge propagation inside the actuator. Notably, the CV curve area of the designed actuator was much larger in comparison with that of the SCN/MFC-IL actuator. Figure 3d and f shows the specific capacitances of the SCN/MFC-IL and SCN/MFC-IL-GN actuators under different scan rates and

applied voltages. The specific capacitances of the SCN/MFC-IL-GN (0.1wt%) ($114.38 \text{ mF cm}^{-2}$) and SCN/MFC-IL-GN(0.05wt%) (89.31 mF cm^{-2}) actuators were much larger than those of the SCN/MFC-IL (81.77 mF cm^{-2}) actuator under $\pm 1.5 \text{ V}$ peaks at a scan rate of 50 mV/s. Especially, the specific capacitances of the SCN/MFC-IL-GN (0.1wt%) actuator were better than those of the SCN/MFC-IL-GN (0.05wt%) and SCN/MFC-IL actuators at various scan rates. As the scan rate increased from 50 to 200 mV/s, the specific capacitance of all three actuators decreased, owing to ions of IL not having sufficient time toward PEDOT:PSS electrodes. The enhanced specific capacitances and CV responses of the designed actuator facilitated fast and easy ion movement within the composite membrane. These

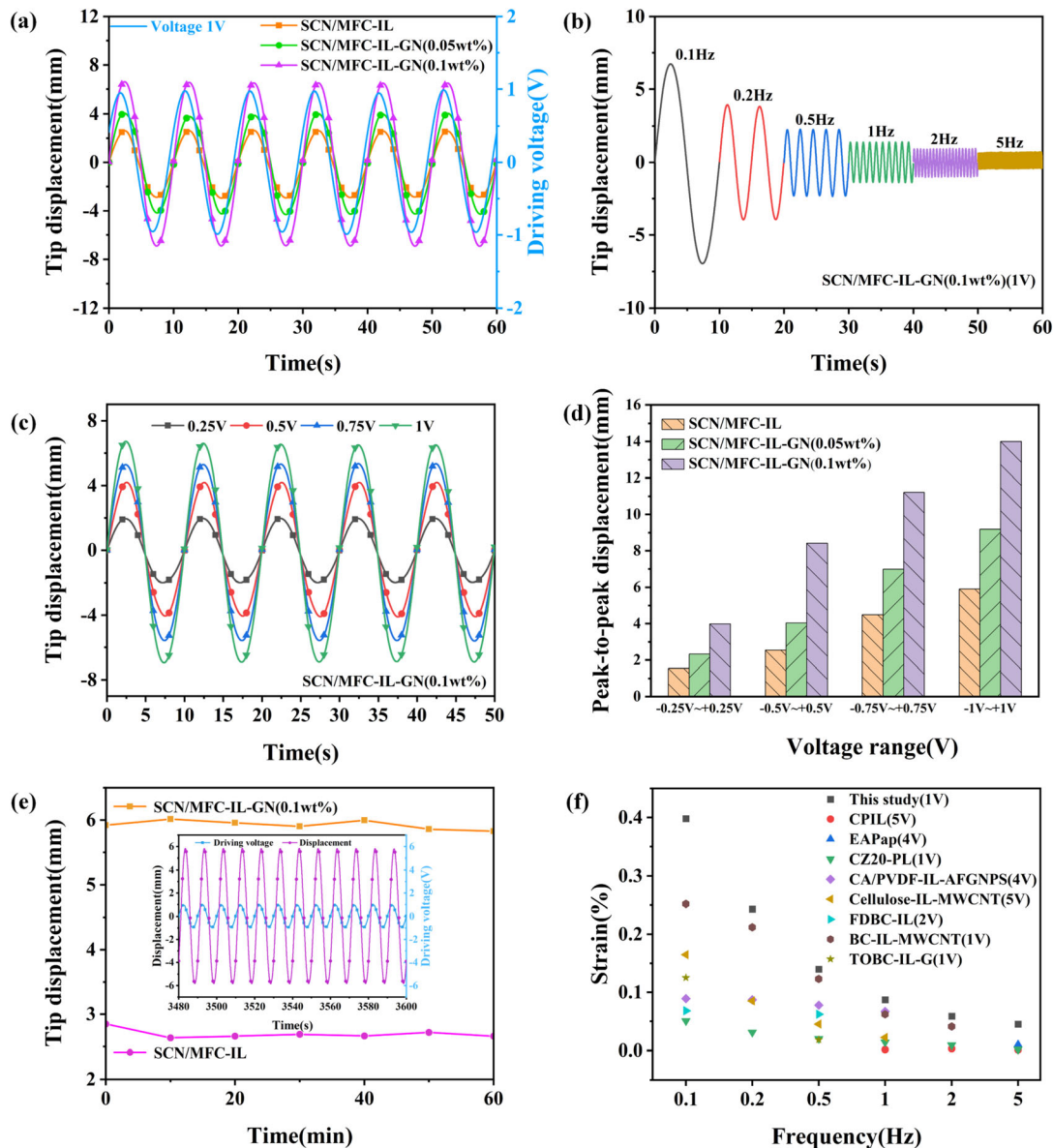


Figure 4 **a** Tip displacements of the SCN/MFC-IL-GN actuators under ± 1.0 V sinusoidal input signal at 0.1 Hz. **b** Tip displacements of the actuators at different frequencies. **c** Tip displacements of the SCN/MFC-IL-GN (0.1wt%) actuator under different input voltages (0.25–1 V) at 0.1 Hz. **d** Peak-to-peak

enhancements were mainly owing to the strong crosslinking and ionic interactions of SCN/MFC composite fibers with IL and GN.

Actuation performances

We further investigated actuation performances of the proposed actuators under various electrical input signals. Figure 4a displays the tip displacements of the SCN/MFC-IL, SCN/MFC-IL-GN (0.05wt%), and

displacements of the three actuators under different input voltages (0.25–1 V) at 0.1 Hz. **e** Displacement of the actuator under a long actuation movement. **f** Comparison of generated strains with other ionic actuators.

SCN/MFC-IL-GN (0.1wt%) actuators under ± 1.0 V sinusoidal input signal at 0.1 Hz. Obviously, the peak displacement of the SCN/MFC-IL-GN (0.1wt%) actuator was about ± 6.6 mm, which was 2.5 and 1.6 times than those of the SCN/MFC-IL (± 2.6 mm) and SCN/MFC-IL-GN (0.05wt%) actuators (± 4.1 mm), respectively. The SCN/MFC-IL-GN actuator demonstrated better bending displacement compared with the SCN/MFC-IL actuator, resulting from the

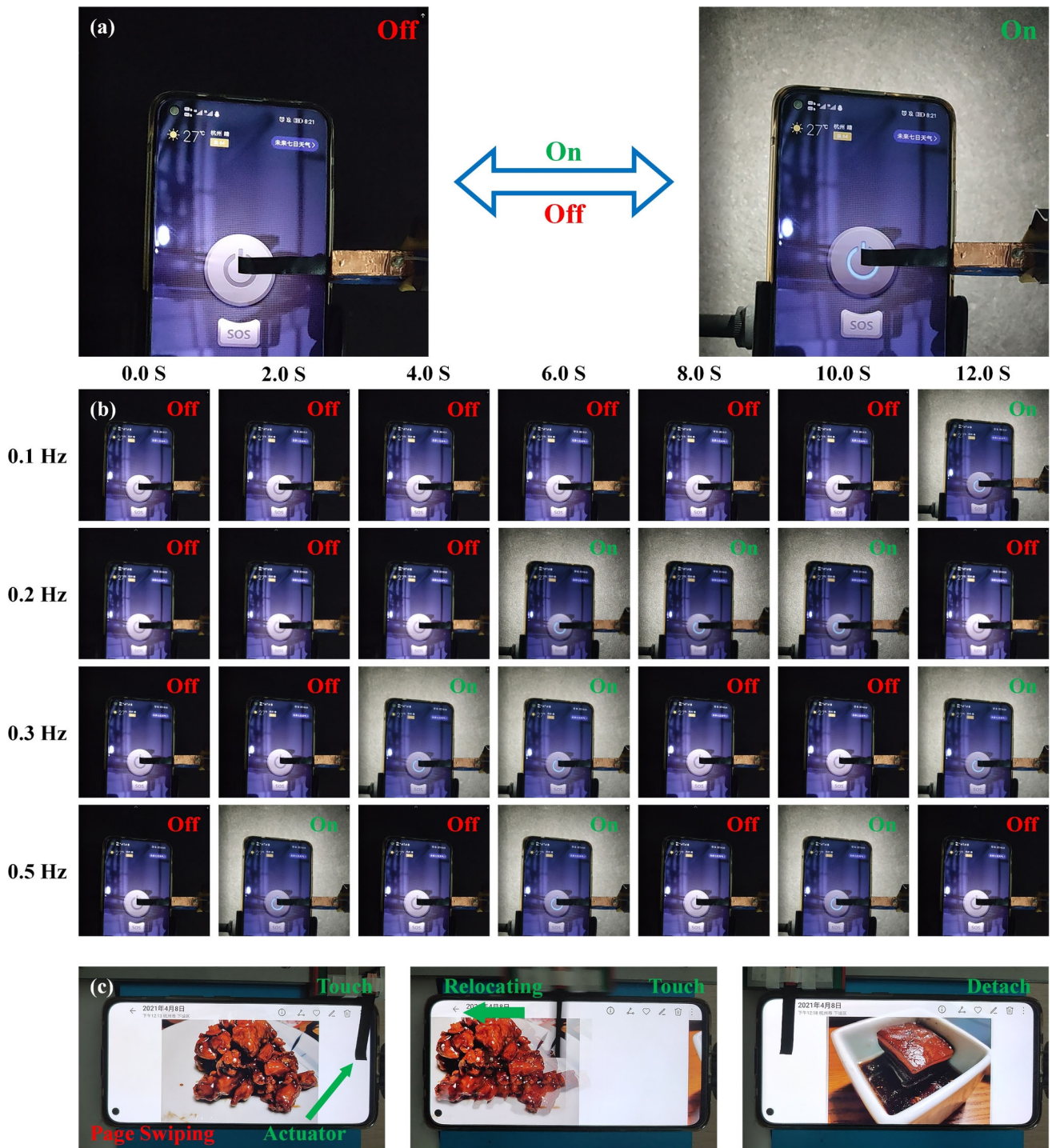


Figure 5 Soft touch robotic finger based on the SCN/MFC-IL-GN actuators. **a-b** Turning on and off the flashlight on a smart phone screen. **b** Operating under various applied frequencies. **c** Sliding electronic photographs on a smart phone screen.

strong crosslinking and ionic interactions among sulfonated groups of SCN, hydroxyl groups of MFC, IL, and GN. Figure 4b displays the tip displacements of the SCN/MFC-IL-GN (0.1wt%) actuator under ± 1.0 V sinusoidal input signal at different frequencies.

This actuator exhibited the best peak displacement at 0.1 Hz. However, as the driving frequency increased, the peak displacement gradually decreased owing to IL not having sufficient time to the electrodes. More interestingly, the peak displacement of the actuator

could reach 0.56 mm when the operational frequency was as high as 5 Hz. The tip displacements were also tested under 0.1 Hz at different voltages, as shown in Fig. 4c and d. Evidently, the tip displacements of the actuators increased with the driving voltage increasing. This indicated that the bending displacement was affected by the actuation voltage, owing to the ion transport inside the membrane highly dependent on the potential field. Surprisingly, when the driving voltage was as low as 0.25 V, the peak displacement of the actuator was up to 1.98 mm. Therefore, the designed actuator demonstrated larger bending displacement under ultralow driving voltage and wide operational frequency. We further investigated the actuation bending mechanism of the actuator. When the actuation voltage was applied to electrode layers, the smaller size anions and larger cations within the membrane moved the anode and cathode sides. Then, the accumulation of these ions at electrode layers led to a relative volume difference, resulting in a mechanical bending deformation.

Furthermore, for practical applications, ionic soft actuators are required to have a long actuation movement. Therefore, the actuation durability of the designed actuator was measured for 1 h under ± 2.0 V sinusoidal input signal at 0.1 Hz, as seen in Fig. 4e. Interestingly, the SCN/MFC-IL-GN (0.1wt%) actuator did not demonstrate actuation response distortion and apparent displacement degradation, and this actuator could retain about 96.7% of initial peak bending displacement, indicating it has excellent actuation durability. These results demonstrated that the designed actuator was able to offer easy-fast conduction path for ion migration in long actuation movement. Ultimately, we compared the bending strains and response time of the actuator with other ionic actuators under various driving frequencies, as shown in Fig. 4f and Table S1 (Supporting Information). Remarkably, the designed actuator presented a remarkable large bending strain (0.398%) and faster response time (0.72 s) under AC 1.0 V at 0.1 Hz compared with other ionic actuators [3, 8, 26–28, 40–42]. The enhanced actuation performances were attributed to the improved electrochemical properties, resulting from the strong crosslinking and ionic interactions among SCN, MFC, IL, and GN.

Additionally, we investigated the bioinspired applications based on the SCN/MFC-IL-GN actuators. The designed ionic soft actuator could imitate

the human finger's behaviors, and it was suitable for the human–robot interaction. As shown in Fig. 5a and b, the bionic finger was driven under 1 V at different frequencies (Movie S1, Supplementary Material). After the voltage was applied, the bionic finger showed bending deformation and touched the screen of the mobile phone to accurately turn on and off the flashlight, showing the fast response and controllability of the bionic finger. Furthermore, as seen in Fig. 5c, we employed the designed actuator under a 1.0 V step stimulation to slide electronic photographs on a mobile phone screen (Movie S2, Supplementary Material). One end of the bionic finger was fixed on a moving stage. Then, the motor drove the guide rail to move, making the actuator sliding electronic photographs. Obviously, the designed actuator could imitate human finger's touching behaviors without damaging the fragile phone screens. We anticipate that these artificial soft fingers can do more complex tasks if they are controlled by a designed or complex circuits.

Conclusions

In summary, we developed a low-voltage high-performance electro-ionic soft actuator based on SCN/MFC, IL, and GN. The designed actuator displayed a large peak displacement (6.6 mm under 1 V at 0.1 Hz), wide actuation frequency (0.1 to 5.0 Hz), low driving voltage (< 1 V), and long actuation movement (96.7% retention for 1 h). The enhanced actuation performances were due to the strong crosslinking and ionic interactions among sulfonated groups of SCN, hydroxyl groups of MFC, IL, and GN. Furthermore, we successfully employed this designed actuator to imitate the human finger's behaviors such as turning on and off the flashlight, and sliding the electronic photographs on smart phone screens. By exploiting these remarkable features, the designed SCN/MFC-IL-GN soft actuators have significant potential for soft robots, haptic devices, biomimetic robots, and implantable biomedical devices.

Acknowledgements

This work was supported by the National Natural Science Foundation of China (51905487), Natural

Science Foundation of Zhejiang Province (LY21E050023), and the Science Foundation of Zhejiang Sci-Tech University (ZSTU) (18022220-Y).

Funding

National Natural Science Foundation of China, 51905487, Fan Wang, Natural Science Foundation of Zhejiang Province, LY21E050023, Fan Wang

Data availability

Data will be made available on request.

Declarations

Conflict of interests The authors declare no conflict of interest.

Ethics declaration The authors declare that this article does not contain any studies with human participants or animals performed by any of the authors.

Supplementary Information: The online version contains supplementary material available at <http://doi.org/10.1007/s10853-022-08061-3>.

References

- [1] Rus DL, Tolley MT (2015) Design, fabrication and control of soft robots. *Nature* 521(7553):467–475
- [2] Nan M, Wang F, Kim S, Li H, Jin Z, Bang D, Kim C-S, Park J-O, Choi E (2019) Ecofriendly high-performance ionic soft actuators based on graphene-mediated cellulose acetate. *Sens Actuators B Chem* 301:127127
- [3] Nan M, Bang D, Zheng S, Go G, Darmawan BA, Kim S, Li H, Kim C-S, Hong A, Wang F, Park J-O, Choi E (2020) High-performance biocompatible nanobiocomposite artificial muscles based on ammonia-functionalized graphene nanoplatelets–cellulose acetate combined with PVDF. *Sens Actuators B Chem* 323:128709
- [4] Wang F, Li Q, Park J-O, Zheng S, Choi E (2021) Ultralow voltage high-performance bioartificial muscles based on ionically crosslinked polypyrrole-coated functional carboxylated bacterial cellulose for soft robots. *Adv Funct Mater* 31(13):2007749
- [5] Wang Y, Niu W, Zhang S, Ju B (2020) Solvent responsive single-material inverse opal polymer actuator with structural color switching. *J Mater Sci* 55(2):817–827
- [6] Wang X, Zhou H, Kang H, Au W, Chen C (2021) Bio-inspired soft bistable actuator with dual actuations. *Smart Mater Struct* 30(12):125001
- [7] Chang K-T, Liu C-Y, Liu J-H (2021) Bioinspired thermal/light-tunable actuators based on predesigned tilted liquid crystal actuators. *J Mater Sci* 56:12350–12363. <https://doi.org/10.1007/s10853-021-06107-6>
- [8] Wang F, Jin Z, Zheng S, Li H, Cho S, Kim HJ, Kim S-J, Choi E, Park J-O, Park S (2017) High-fidelity bioelectronic muscular actuator based on porous carboxylate bacterial cellulose membrane. *Sens Actuators B* 250:402–411
- [9] Hu Y, Lian H, Zu L, Jiang Y, Hu Z, Li Y, Shen S, Cui X, Liu Y (2016) Durable electromechanical actuator based on graphene oxide with in situ reduced graphene oxide electrodes. *J Mater Sci* 51(3):1376–1381. <https://doi.org/10.1007/s10853-015-9456-4>
- [10] Bian C, Zhu Z, Bai W, Chen H, Li Y (2020) Fast actuation properties of several typical IL-based ionic electro-active polymers under high impulse voltage. *Smart Mater Struct* 29(3):035014
- [11] Wang F, Jeon J-H, Kim S-J, Park J-O, Park S (2016) An eco-friendly ultra-high performance ionic artificial muscle based on poly(2-acrylamido-2-methyl-1-propanesulfonic acid) and carboxylated bacterial cellulose. *J Mater Chem B* 4(29):5015–5124
- [12] Acerce M, Akdogan E, Chhowalla M (2017) Metallic molybdenum disulfide nanosheet-based electrochemical actuators. *Nature* 549(7672):370–373
- [13] Altinkaya E, Seki Y, Yılmaz Ö, Çetin L, Özdemir O, Sen I, Sever K, Gürses B, Sarikanat M (2016) Electromechanical performance of chitosan-based composite electroactive actuators. *Compos Sci Technol* 129:108–115
- [14] Pagoli A, Chapelle F, Corrales-Ramon J-A, Mezouar Y, Lapusta Y (2021) Review of soft fluidic actuators: classification and materials modeling analysis. *Smart Mater Struct* 31(1):013001
- [15] Ma S, Zhang Y, Liang Y, Ren L, Tian W, Ren L (2020) High-performance ionic-polymer-metal composite: toward large-deformation fast-response artificial muscles. *Adv Funct Mater* 30(7):1908508
- [16] Sudhawiyangkul T, Yoshida K, Eom SI, Kim J-W (2021) A multi-DOF soft microactuator integrated with flexible electro-rheological microvalves using an alternating pressure source. *Smart Mater Struct* 30(8):085006
- [17] Wang F, Huang D, Li Q, Wu Y, Yan B, Wu Z, Park S (2023) Highly electro-responsive ionic soft actuator based on

- graphene nanoplatelets-mediated functional carboxylated cellulose nanofibers. *Compos Sci Technol* 231:109845
- [18] Han J, Jiang W, Zhang H, Zhang Y, Feng X, Wang L, Niu D, Lei B, Liu H (2020) Untethered, ultra-light soft actuator based on positively charged 3D fluffy silica micro-nanofibers by electrospinning. *J Mater Sci* 55(27):12789–12800. <https://doi.org/10.1007/s10853-020-04944-5>
- [19] Wang F, Kong Y, Shen F, Wang Y, Wang D, Li Q (2022) High-performance microfibrillated cellulose-based low voltage electroactive ionic artificial muscles in bioinspired applications. *Compos Part B-Eng* 228:109436
- [20] Umrao S, Tabassian R, Kim J, Nguyen VH, Zhou Q, Nam S, Oh I-K (2019) MXene artificial muscles based on ionically cross-linked $Ti_3C_2T_x$ electrode for kinetic soft robotics. *Sci Robot* 4(33):eaaw7797
- [21] Valentine A, Busbee T, Boley J, Raney J, Chortos A, Kotikian A, Berrigan J, Durstock M, Lewis J (2017) Hybrid 3D printing of soft electronics. *Adv Mater* 29(40):1703817
- [22] Wu G, Wu X, Xu Y, Cheng H, Meng J, Yu Q, Shi X, Zhang K, Chen W, Chen S (2019) High-performance hierarchical black-phosphorous-based soft electrochemical actuators in bioinspired applications. *Adv Mater* 31(25):1806492
- [23] Wang F, Wang L, Wang Y, Wang D (2022) Highly bendable ionic electroactive polymer actuator based on carboxylated bacterial cellulose by doping with MWCNT. *Appl Phys A-Mater* 128:911
- [24] Liu Z, Liu YD, Shi Q, Liang Y (2021) Electroactive dielectric polymer gels as new-generation soft actuators: a review. *J Mater Sci* 56(27):14943–14963. <https://doi.org/10.1007/s10853-021-06260-y>
- [25] Kim J, Yun S, Ounaies Z (2006) Discovery of cellulose as a smart material. *Macromolecules* 39:4202–4206
- [26] Kim S-S, Jeon J-H, Kee C-D, Oh I-K (2013) Electro-active hybrid actuators based on freeze-dried bacterial cellulose and PEDOT:PSS. *Smart Mater Struct* 22(8):085026
- [27] Maha De Va S-K, Kim J (2010) An electro-active paper actuator made with cellulose–polypyrrole–ionic liquid nanocomposite: influence of ionic liquid concentration, type of anion and humidity. *Smart Mater Struct* 19(10):105014
- [28] Wang N, Yi C, Kim J (2007) Electroactive paper actuator made with chitosan-cellulose films: effect of acetic acid. *Macromol Mater Eng* 292(6):748–753
- [29] Hong C-H, Ki S-J, Jeon J-H, Che H-L, Park I-K, Kee C-D, Oh I-K (2013) Electroactive bio-composite actuators based on cellulose acetate nanofibers with specially chopped polyaniline nanoparticles through electrospinning. *Compos Sci Technol* 87:135–141
- [30] Liu S, Tao D, Bai H, Liu X (2012) Cellulose-nanowhisker-templated synthesis of titanium dioxide/cellulose nanomaterials with promising photocatalytic abilities. *J Appl Polym Sci* 126(51):E282–E290
- [31] Dadkhah Tehrani A, Neysi E (2013) Surface modification of cellulose nanowhisker throughout graft polymerization of 2-ethyl-2-oxazoline. *Carbohydr Polym* 97(1):98–104
- [32] Siró I, Plackett D (2010) Microfibrillated cellulose and new nanocomposite materials: a review. *Cellulose* 17(3):459–494
- [33] Lavoine N, Desloges I, Dufresne A, Bras J (2012) Microfibrillated cellulose-Its barrier properties and applications in cellulosic materials: a review. *Carbohydr Polym* 90(2):735–764
- [34] Geim A-K (2009) Graphene: status and prospects. *Science* 324(5934):1530–1534
- [35] Zuchowska A, Chudy M, Brzózka Z, Dybko A (2017) Graphene as a new material in anticancer therapy-in vitro studies. *Sens Actuators B Chem* 243:152–165
- [36] Stankovich S, Dikin D-A, Dommett G, Kohlhaas K-M, Zimney E-J, Stach E-A, Piner R-D, Nguyen S-T, Ruoff R-S (2006) Graphene-based composite materials. *Nature* 442(7100):282–286
- [37] Cheedarala R-K, Jeon J-H, Kee C-D, Oh I-K (2015) Bio-inspired all-organic soft actuator based on a π - π stacked 3D ionic network membrane and ultra-fast solution processing. *Adv Funct Mater* 24(38):6005–6015
- [38] Wang F, Kim H, Park S, Kee C, Kim S, Oh IK (2016) Bendable and flexible supercapacitor based on polypyrrole-coated bacterial cellulose core-shell composite network. *Compos Sci Technol* 128:33–40
- [39] Rasouli H, Naji L, Hosseini M-G (2017) The effect of MWCNT content on electropolymerization of PPy film and electromechanical behavior of PPy electrode-based soft actuators. *J Electroanal Chem* 806:136–149
- [40] Yang L, Sun Z, Li F, Du S, Song W (2019) Performance enhancement of cellulose-based biocomposite ionic actuator by doping with MWCNT. *Appl Phys A* 125(8):547
- [41] Kim S-S, Jeon J-H, Kim H-I, Kee C-D, Oh I-K (2015) High-fidelity bioelectronic muscular actuator based on graphene-mediated and TEMPO-oxidized bacterial cellulose. *Adv Func Mater* 25(23):3560–3570
- [42] Wang Y, Wang F, Kong Y, Wang L, Li Q (2021) Novel ionic bioartificial muscles based on ionically crosslinked multi-walled carbon nanotubes-mediated bacterial cellulose membranes and PEDOT:PSS electrodes. *Smart Mater Struct* 31(2):025023

Publisher's Note Springer Nature remains neutral with regard to jurisdictional claims in published maps and institutional affiliations.

Springer Nature or its licensor (e.g. a society or other partner) holds exclusive rights to this article under a publishing agreement with the author(s) or other

rightsholder(s); author self-archiving of the accepted manuscript version of this article is solely governed by the terms of such publishing agreement and applicable law.